

**STUDY OF Ge AND GeO<sub>2</sub> LOW DIMENSIONAL STRUCTURES  
SYNTHESIZED BY ELECTROCHEMICAL DEPOSITION FOR  
SENSING APPLICATIONS**

**MOHAMMED J. JAWAD**

**UNIVERSITI SAINS MALAYSIA**

**2015**

**STUDY OF Ge AND GeO<sub>2</sub> LOW DIMENSIONAL STRUCTURES  
SYNTHESIZED BY ELECTROCHEMICAL DEPOSITION FOR  
SENSING APPLICATIONS**

**By**

**MOHAMMED J. JAWAD**

**Thesis submitted in fulfillment of the requirements  
for the degree of Doctor of philosophy**

**April 2015**

## ACKNOWLEDGEMENTS

On this memorable night in my life when I am going to finish the writing of this thesis, first of all I bestowed the thanks to Allah Almighty for granting me health with capability to complete this research work. I dedicated this thesis to the soul of my father, God have mercy on him. Along the way to the completion of this thesis, my family, my wife, my son Taha, sisters, and my brother all contributed in different ways. At this moment I am very thankful to all of them.

I would like to express my deep sense of gratitude to my supervisor Prof. Dr. Md Roslan Hashim for his useful and valuable suggestions, inspiring guidance and consistent encouragement without which this thesis could have never been materialized. He always taught me how to face hard moments in this research.

I also wish to record my sincere thanks to my co-supervisor Dr. Nihad K. Ali AL-Obaidi for his kind cooperation, valuable contribution, patience and guidance during my study and research work.

To be fair I had to extend my sincere thanks to all of NOR lab staff for the cooperation and kindness behaviors with all the postgraduate students. I also thank all my friends and colleagues who supported me and helped me at the School of Physics, Universiti Sains Malaysia.

## TABLE OF CONTENTS

	<b>PAGE</b>
<b>ACKNOWLEDGEMENTS</b>	ii
<b>TABLE OF CONTENTS</b>	iii
<b>LIST OF TABLES</b>	vii
<b>LIST OF FIGURES</b>	viii
<b>LIST OF SYMBOLS</b>	xii
<b>LIST OF ABBREVIATIONS</b>	xiv
<b>ABSTRAK</b>	xv
<b>ABSTRACT</b>	xvii
<b>CHAPTER 1: INTRODUCTION</b>	
1.1 Historical overview	1
1.2 Problem statements	4
1.3 Research objectives	5
1.4 Originality of the research work	6
1.5 Outlines of the thesis	6
<b>CHAPTER 2: LITERATURE REVIEW AND THEORETICAL BACKGROUND</b>	
2.1 Introduction	8
2.2 Overview of semiconductors nanostructure	8
2.3 Overview of Ge nanostructure growth techniques	13
2.3.1 Chemical vapour deposition (CVD)	14
2.3.2 Molecular beam epitaxy (MBE)	15
2.3.3 Atomic layer epitaxy (ALE)	16
2.3.4 Electrochemical deposition (ECD)	17
2.4 Properties of Ge	20
2.4.1 Crystal structure of Ge	20
2.4.2 Physical properties of Ge	22
2.4.3 Germanium dioxide (GeO <sub>2</sub> ) properties	22
2.5 Principles of electrochemical deposition (ECD) technique	24

2.5.1	Faraday's law and mass transfer	25
2.5.2	Current density	27
2.5.3	Electrodes and electrode potential	27
2.5.4	Electrolyte solution for ECD technique	29
2.6	Mechanisms of the reactions to form Ge and GeO <sub>2</sub> nanostructures	30
2.6.1	Mechanisms for growth of Ge nanostructures by ECD technique	30
2.6.2	Mechanism for growth of GeO <sub>2</sub> nanostructures by ECD technique	32
2.7	MSM photodetector based on Ge nanostructures	32
2.7.1	Responsivity	35
2.7.2	Quantum efficiency	36
2.7.3	Response time	36
2.8	Hydrogen gas sensor based on GeO <sub>2</sub>	37
2.8.1	Sensitivity	39
2.8.2	Response and recovery times	39
<b>CHAPTER 3: EXPERIMENTAL PROCEDURES</b>		
3.1	Introduction	40
3.2	Substrate cleaning and preparation	40
3.2.1	Silicon substrate	42
3.2.2	Porous silicon substrate	42
3.3	The cells and electrolyte solutions	43
3.3.1	Electrolyte preparation cell for Ge	43
3.3.2	Electrochemical deposition cell	44
3.3.3	Electrolyte solution for Ge deposition	45
3.3.4	Electrolyte solution for GeO <sub>2</sub> deposition	46
3.4	Synthesis of Ge nanostructures by ECD technique	46
3.4.1	Effect of current density	46
3.4.2	Effect of different deposition durations	47
3.4.3	Synthesis of Ge nanostructures on different substrates	47

3.5	Synthesis of GeO <sub>2</sub> nanostructures by ECD technique	47
3.6	Characterization	48
3.6.1	Scanning electron microscope (SEM) and energy dispersive X-ray (EDX)	48
3.6.2	High resolution X-ray diffraction (HR-XRD)	49
3.6.3	Photoluminescence (PL) and Raman spectroscopy	52
3.7	Metal contacts for device fabrication	53
3.7.1	RF magnetron sputtering	53
3.7.2	Annealing tube furnace	55
3.7.3	Measurements of current-voltage characteristics	55
3.8	MSM photodetector based on Ge-like microflowers	56
3.9	MSM UV detector based on Ge and GeO <sub>2</sub> microstructures	57
3.10	Hydrogen gas sensor based on GeO <sub>2</sub>	57

#### **CHAPTER 4: STUDY OF ELECTROCHEMICAL DEPOSITION OF Ge MICROSTRUCTURES**

4.1	Introduction	59
4.2	Growth of Ge microstructures on Si substrate at different current densities	59
4.2.1	Surface morphology analysis	59
4.2.2	X-ray diffraction analysis	61
4.2.3	Raman analysis	64
4.2.4	Photoluminescence analysis	66
4.3	Growth of Ge microstructures on Si substrate for different durations	69
4.3.1	Surface morphology analysis	69
4.3.2	X-ray diffraction analysis	71
4.3.3	Raman analysis	74
4.4	Comparative study of Ge microstructures grown on different substrates	76
4.4.1	Surface morphology analysis	76
4.4.2	X-ray diffraction analysis	78

4.4.3 Raman analysis	81
4.5 MSM photodetector based on Ge-like microflowers	83
4.5.1 Effect of thermal annealing temperatures on MSM photodetector based on Ge-like microflowers in the dark mode	85
4.5.2 Effect of thermal annealing temperatures on MSM photodetector based on Ge-like microflowers under white and UV illuminations	87
4.5.3 Photo-response time of the MSM photodetector based on Ge-like microflowers	89
4.6 Summary	93
<b>CHAPTER 5: THE STUDY OF ELECTROCHEMICAL DEPOSITION OF GeO<sub>2</sub> MICROSTRUCTURES</b>	
5.1 Introduction	95
5.2 Synthesis of GeO <sub>2</sub> microstructure on PS by using ECD technique	95
5.2.1 Surface morphology analysis	95
5.2.2 X-ray diffraction analysis	97
5.2.3 Raman analysis	99
5.2.4 Photoluminescence analysis	101
5.3 Comparative study of the MSM UV detector based on GeO <sub>2</sub> and Ge microstructures grown on PS	103
5.4 Hydrogen gas sensor based on GeO <sub>2</sub>	106
5.5 Summary	114
<b>CHAPTER 6: CONCLUSIONS AND FUTURE OUTLOOK</b>	
6.1 Conclusions	116
6.2 Future work	117
<b>REFERENCES</b>	119
<b>APPENDICES</b>	133
APPENDIX A: Physical properties of Ge and GeO <sub>2</sub>	133
APPENDIX B: Metal-semiconductor interface	134
<b>LIST OF PUBLICATIONS</b>	137

## LIST OF TABLES

		<b>PAGE</b>
Table 4.1	Full width at half maximum (FWHM) intensity, $d$ -spacing, lattice constant $a$ , average size of the crystals $D$ and in-plane strain $\epsilon_a$ determined for the Ge samples deposited at different current density. In this table all parameters of sample C are similar to those of sample D.	63
Table 4.2	$d$ -spacing, FWHM, lattice constant, average crystallite size $D$ , elastic strain $\epsilon_a$ and film thickness determined for the Ge samples deposited at different durations.	73
Table 4.3	$d$ -spacing and lattice constant of bulk Ge, also, $d$ -spacing, lattice constant, FWHM, average crystallite size and strain ( $\epsilon_a$ ) for as-grown Ge on Si and PS substrates.	81
Table 4.4	Barrier height, ideality factor, series resistance, contrast ratio and current gain for as grown and annealed MSM photodetectors measured under white light and UV illuminations.	88
Table 5.1	Plane, diffraction angle, $d$ -spacing, FWHM, lattice parameters $a$ and $c$ and crystallite size $D$ for the GeO <sub>2</sub> samples deposited at current density of 5 (sample C) and 10 mA/cm <sup>2</sup> (sample D).	99
Table 5.2	Barrier height, current at 5V, contrast ratio at 5V, leakage current at -1V, series resistance and the gain for photodetectors based on Ge and GeO <sub>2</sub> microstructures grown on PS.	105
Table 5.3	Barrier height, ideality factor and series resistance for the sensor based on hexagonal GeO <sub>2</sub> at different H <sub>2</sub> flow rates.	108

## LIST OF FIGURES

		<b>PAGE</b>
Figure 2.1	Schematic of the low-dimensional structure and the density of state (DOS) as a function of the energy for a particle controlled to move in the bulk (a), in a quantum well (b), in quantum wire (c), and quantum dot (d) [adopted from Hens et al., 2002].	9
Figure 2.2	Diamond lattice structure [adopted from Sze, 1985].	20
Figure 2.3	Miller indices of some important planes in a cubic crystal [adopted from Sze and Ng, 2008].	21
Figure 2.4	Band structure of germanium [adopted from Sze, 1985]	22
Figure 2.5	Electrochemical cell [adopted from Paunovic and Schlesinger, 1998].	25
Figure 2.6	A schematic image of an MSM photodiode structure.	33
Figure 2.7	Energy band diagram of (a) Schottky photodetector and (b) MSM photodetector at zero bias and (c) MSM photodetector at moderate bias.	34
Figure 3.1	Experimental procedures flowchart.	41
Figure 3.2	The photoelectrochemical etching experimental set up used to fabricate PS (a) homemade quarter cylinder Teflon cell and (b) the schematic drawing of the photoelectrochemical etching set up.	42
Figure 3.3	Schematic diagram of electrochemical etching cell for Ge target.	44
Figure 3.4	Electrochemical deposition cell (a) photograph and (b) schematic diagram.	45
Figure 3.5	(a) Scanning electron microscope (SEM) for high magnification optical observation and energy dispersive X-ray (EDX), (b) schematic diagram [adopted from Reimer and Hawkes, 1988].	49
Figure 3.6	High resolution XRD (a) photograph (b) schematic diagram.	50
Figure 3.7	Reflection of X-rays from two planes of atoms in a solid	50
Figure 3.8	(a) RF-sputtering equipment and (b) schematic diagram of the system [adopted from Chen et al., 2004].	54
Figure 3.9	(a) Annealing tube furnace equipment and (b) schematic diagram of furnace.	55

Figure 3.10	The metal mask used in the fabrication of the MSM photodetector.	56
Figure 3.11	The schematic diagram of hydrogen gas sensing system and gas chamber.	58
Figure 4.1	SEM images and EDX spectra of the Ge electrochemically deposited on Si (100). Samples A, B, C, D, E, and F were prepared by applying different current densities 7.5, 6, 5, 4, 3 and 2 mA/cm <sup>2</sup> , respectively, for two hours at room temperature.	60
Figure 4.2	XRD patterns of Ge (a) for samples A, B, C, and D and (b) for samples E and F, where the applied current densities were 7.5, 6, 5, 4, 3 and 2 mA/cm <sup>2</sup> , respectively, illustrating the preferred crystallographic orientations of the Ge as grown on Si substrates.	61
Figure 4.3	Raman spectra of the deposited Ge samples, at current density of (A) 7.5, (B) 6, (C) 5, (D) 4, (E) 3 and (F) 2 mA/cm <sup>2</sup> .	64
Figure 4.4	PL spectra of the deposited Ge samples, (a) at current density of (A) 7.5, (B) 6, (C) 5 and (D) 4 mA/cm <sup>2</sup> , (b) at current density of (E) 3 and (F) 2 mA/cm <sup>2</sup> .	67
Figure 4.5	The FESEM images A, B, C and D of Ge grown on Si for deposition times 0.5, 1, 1.5 and 2 h, respectively. The EDX spectrum is represented by E.	70
Figure 4.6	XRD patterns of Ge samples deposited for different durations: A for 0.5 h, B for 1 h, C for 1.5 h and D for 2 h.	72
Figure 4.7	(a) Variation of film thickness with deposition time and the variation of lattice constant with film thickness, (b) variation of lattice constant <i>a</i> , average crystallite size <i>D</i> of crystalline Ge with deposition time.	73
Figure 4.8	Raman spectra of Ge films deposited for different durations, A for 0.5 h, B for 1 h, C for 1.5 h and D for 2 h and bulk c-Ge included for comparison.	74
Figure 4.9	SEM images (a) surface of PS sample, (b) cross section of PS sample, (c) low and (d) high magnification SEM images of Ge microrods on Si, (e) microspheres with nanowires in low magnification and (f) high magnification of Ge nanowires on PS.	77
Figure 4.10	XRD pattern of Ge films grown on Si and PS.	79
Figure 4.11	Enlarged XRD (111) peak of Ge films for (a) Ge on Si substrate and (b) Ge on PS substrate.	80

Figure 4.12	Typical Raman spectra of Ge films mode grown on PS and Si substrates.	82
Figure 4.13	I-V characteristics of the as grown MSM photodetector based on Ge-like microflowers under dark, white light and UV illuminations.	84
Figure 4.14	I-V characteristics of the MSM photodetector, (a) linear and (b) logarithmic forward and reverse bias, at different annealing temperatures: as-deposited, 100°C, 200°C and 300°C in the dark mode.	85
Figure 4.15	The dependence of Schottky barrier height on annealing temperature for the MSM photodetector.	86
Figure 4.16	A graphical representation of the ideality factor as a function of annealing temperature for the MSM photodetector.	87
Figure 4.17	I-V characteristics of the MSM photodetector at different annealing temperatures under (a) white light (b) UV illumination.	87
Figure 4.18	I-V characteristics (a) and the current gain (b) for the MSM photodetector annealed at 200°C in the dark, white and UV environment.	90
Figure 4.19	Spectral responsivity of the MSM photodetector based on Ge-like microflowers at room temperature and 5V applied bias.	91
Figure 4.20	Transient response of the MSM photodetector to 405 nm and 460 nm illumination under 3V bias voltage.	92
Figure 4.21	An enlargement of typical signal showing rise and fall times for photodetector illuminated by 405 nm and 460 nm wavelengths.	92
Figure 5.1	SEM images of as prepared porous silicon A, GeO <sub>2</sub> chemically deposited B, electrochemically deposited GeO <sub>2</sub> at current density of 5 mA/cm <sup>2</sup> C, and at current density of 10 mA/cm <sup>2</sup> D. At the right side of B, C and D are their respective EDX spectrum.	96
Figure 5.2	XRD patterns of crystalline GeO <sub>2</sub> grown on PS for sample C with 5 mA/cm <sup>2</sup> and sample D with 10 mA/cm <sup>2</sup> .	98
Figure 5.3	Raman spectra of as-prepared PS as sample A, GeO <sub>2</sub> powder on PS as sample B, and GeO <sub>2</sub> electrochemically deposited on PS as sample D. A spectrum of c-Si is included for comparison.	100

Figure 5.4	PL spectra of as-prepared PS as sample A, GeO <sub>2</sub> powder chemically deposited on PS as sample B, and GeO <sub>2</sub> electrochemically deposited on PS as sample D.	101
Figure 5.5	Logarithmic variation of current $I$ with applied voltage $V$ measured at room temperature for the representative two diodes based on GeO <sub>2</sub> and Ge grown on PS in the dark and UV illumination.	104
Figure 5.6	Current gain of the MSM UV photodetectors based on Ge and GeO <sub>2</sub> grown on PS.	106
Figure 5.7	I-V characteristics in (a) linear and (b) logarithmic plots, measured at room temperature for Pd/GeO <sub>2</sub> before and after H <sub>2</sub> exposure at different flow rates.	107
Figure 5.8	Variation of barrier potential $\phi_b$ with different H <sub>2</sub> flow rates for Pd/GeO <sub>2</sub> Schottky diode on PS.	109
Figure 5.9	Variation of (a) series resistance and (b) ideality factor for the gas sensor with different H <sub>2</sub> flow rates.	109
Figure 5.10	Forward-bias plot of the logarithmic (I-V) characteristic for Pd/GeO <sub>2</sub> gas sensor at different temperatures (a) before gas exposure, (b) after gas exposure at 30 sccm and (c) 60 sccm.	110
Figure 5.11	Variation of (a) barrier height ( $\phi_b$ ) and (b) ideality factor ( $n$ ) with the temperature before and after H <sub>2</sub> exposure for two representatives H <sub>2</sub> flow rates.	111
Figure 5.12	Variation of sensitivity with (a) H <sub>2</sub> flow rate measured at room temperature and (b) temperature for two typical H <sub>2</sub> flow rates 30 and 60 sccm.	112
Figure 5.13	Hydrogen sensing mechanism for the effectively Schottky barrier height variation [adopted from Huang et al., 2007].	113
Figure 5.14	Response behavior of a representative Pd/GeO <sub>2</sub> Schottky diode sensor.	113

## LIST OF SYMBOLS

$\phi_b$	Schottky barrier height
$m_l^*$	Longitudinal effective mass
$m_t^*$	Transversal effective mass
$A$	Area
$A^{**}$	Richardson constant
$a_o$	Unstrained lattice parameter
$D_e$	Density of material
$D$	Crystallite size
$d$	d-spacing
$e$	Electron
$F$	Faraday constant
$h_e$	Hole
$h$	Planck constant
$I$	Current
$I_{air}$	Current in ambient air
$I_{H_2}$	Current with hydrogen flow rate
$I_o$	Saturation current
$I_{ph}$	Photocurrent
$J$	Current density
$k$	Boltzman constant
$M$	Atomic/Molecular weight
$m$	Mass
$m_e$	Effective mass
$N$	Number of mole
$n$	Ideality factor
$N_d$	Doping concentration of the semiconductor
pH	Acidic of solution
$P_{inc}$	Incident optical power
$Q$	Total electrical charge passed through a cell
$q$	Electron charge
$R$	Responsivity
$R_{air}$	Resistance by ambient air exposure
$R_{H_2}$	Resistance by hydrogen exposure
$R_s$	Series resistance
$S$	Sensitivity
$t$	Time
$T$	Temperature
$T_d$	Deposition time
$T_h$	Thickness
$V$	Volume
$V_d$	Voltage across the diode
$\alpha$	Absorption coefficient
$\varepsilon$	Dielectric constant
$\varepsilon_a$	Strain
$\eta$	Quantum efficiency
$\theta_i$	Coverage of hydrogen atoms
$\mu$	Effective dipole moment
$\nu$	Light frequency

$\tau_0$  Time of carrier diffusion to the junction depletion region  
 $\tau_s$  Transit time of carrier drift across the depletion region

## LIST OF ABBREVIATIONS

0D	Zero-dimension nanostructures
1D	One-dimension nanostructures
2D	Two-dimension nanostructures
ALE	Atomic layer epitaxy
BH	Barrier height
CVD	Chemical vapor deposition
DOS	Density of states
ECD	Electrochemical deposition
EDX	Energy dispersive X-ray
e-h	Electron-hole pair
FCC	Face centered cubic
FWHM	Full width at half maximum
HEMTs	High electron mobility transistors
HR-XRD	High resolution X-ray diffraction
IR	Infrared
I-V	Current-Voltage
LEDs	Light-emitting diodes
LO	Longitudinal optical phonons
MBE	Molecular beam epitaxy
MS	Metal-semiconductor
MSM	Metal-semiconductor-metal
NBOHC	Nonbridged oxygen hole center
NIR	Near infra red
PD	Photodetector
PL	Photoluminescence
PS	Porous silicon
QDs	Quantum dots
QWs	Quantum wells
RF	Radio frequency
RTA	Rapid thermal anneal
SEM	Scanning electron microscope
TO	Transversal optical phonons

# **KAJIAN STRUKTUR DIMENSI RENDAH Ge DAN GeO<sub>2</sub> TERSINTESIS MELALUI PEMENDAPAN ELEKTROKIMIA UNTUK APLIKASI PENDERIAAN**

## **ABSTRAK**

Projek ini mencadangkan satu cara alternatif untuk menyediakan struktur mikro-Ge dan GeO<sub>2</sub> tanpa pemangkin dan berkos rendah dengan menggunakan teknik pemendapan elektrokimia (ECD). Pertama sekali, struktur mikro Ge telah disintesis di atas substrat Si dengan mengenakan ketumpatan arus yang berbeza dari 2 ke 7.5 mA/cm<sup>2</sup>. Bentuk morfologi Ge yang dihasilkan menunjukkan pergantungan yang tinggi terhadap ketumpatan arus. Purata saiz kristal dan terikan telah meningkat dengan peningkatan ketumpatan arus. Kesan jangka masa yang berbeza (0.5, 1, 1.5 dan 2 h) ke atas ciri morfologi, struktur dan optik rod mikro kubus Ge yang ditumbuhkan di atas Si telah dikaji. Diperhatikan bahawa ketebalan lapisan Ge meningkat sehingga 3 µm dalam tempoh 2 jam. Perbandingan juga telah dilakukan ke atas struktur mikro Ge yang disintesiskan di atas substrat silikon berlian (PS) dan Si. Hasil kajian menunjukkan bahawa terikan elastik filem Ge pada PS adalah lebih rendah daripada filem Ge pada substrat Si. Ciri-ciri fotoelektrik untuk pengesan foto Pd MSM berasaskan Ge berbentuk seperti bunga sebelum dan selepas suhu penyepuhlindapan 100, 200 dan 300°C dalam pencahayaan gelap, cerah dan ultraungu (UV) telah dikaji. Spektrum masa sambutan mempamerkan dua puncak utama pada 400 dan 500 nm dan kecekapan kuantum adalah 13.6% untuk 400 nm.

Kedua, struktur mikro GeO<sub>2</sub> di atas PS juga telah disintesis pada ketumpatan arus yang berbeza 5 dan 10 mA/cm<sup>2</sup>. Ciri-ciri morfologi, struktur dan optik telah dikaji. Perbandingan telah dibuat untuk pengesan UV berasaskan hasil tinggi penumbuhan struktur mikro Pd/GeO<sub>2</sub> dan Pd/Ge yang ditumbuhkan di atas PS. Didapati bahawa gandaan maksimum adalah 70 untuk Ge/PS dan 600 untuk GeO<sub>2</sub>/PS. Peranti baru

berdasarkan struktur mikro  $\text{GeO}_2/\text{Pd}$  sebagai pengesan  $\text{H}_2$  telah dihasilkan. Keputusan menunjukkan sambutan yang ketara dengan kadar aliran gas  $\text{H}_2$  yang berbeza. Pengesan  $\text{Pd}/\text{GeO}_2$  juga diukur pada suhu yang berbeza 25, 50, 75 dan  $100^\circ\text{C}$ . Kepekaan optimum adalah pada suhu  $25^\circ\text{C}$  dan kepekaan menunjukkan penurunan dengan peningkatan suhu.

# **STUDY OF Ge AND GeO<sub>2</sub> LOW DIMENSIONAL STRUCTURES SYNTHESIZED BY ELECTROCHEMICAL DEPOSITION FOR SENSING APPLICATIONS**

## **ABSTRACT**

The project proposed an alternative way for preparing Ge and GeO<sub>2</sub> nanostructures without catalyst and low cost by using electrochemical deposition (ECD) technique. Firstly Ge microstructures were synthesized on Si at different applied current densities which were varied from 2 to 7.5 mA/cm<sup>2</sup>. The morphologies of Ge showed strong dependence on the applied current density. The average crystal size and the strain were increased with increasing of the current density. The effect of different deposition durations of 0.5, 1, 1.5 and 2 h on the morphological, structural and optical properties of Ge cubic microrods growth on Si was investigated. It was observed that the thickness of Ge layer increased up to 3 μm within duration of 2 h. A comparison between Ge microstructures synthesized on porous silicon (PS) and Si substrates was performed. The results showed that the elastic strain of Ge films grown on PS was lower than that grown on Si substrate. The photoelectric properties of palladium (Pd) metal-semiconductor-metal (MSM) photodetector based on Ge-like microflowers before and after annealing temperatures of 100, 200 and 300°C in dark, white and ultra violet (UV) illumination were investigated. The spectral responsivity exhibited two pronounced peaks at 400 and 500 nm and the quantum efficiency was 13.6 % for 400 nm.

Secondly, GeO<sub>2</sub> microstructures on PS were also synthesized at current density of 5 and 10 mA/cm<sup>2</sup>. The morphological, structural and optical properties of GeO<sub>2</sub> microstructures were inspected. A comparison between UV detector based on Pd/GeO<sub>2</sub> and Pd/Ge microstructures grown on PS was established. It was found that the maximum gain was 70 for Ge/PS and 600 for GeO<sub>2</sub>/PS. Novel device based on

Pd/GeO<sub>2</sub> microstructures as H<sub>2</sub> sensor was demonstrated. The results displayed significant response with different flow rates of H<sub>2</sub> gas. Pd/GeO<sub>2</sub> sensor was also measured at different temperatures of 25, 50, 75 and 100°C. The optimum sensitivity of this sensor was at 25°C and degraded with elevating temperatures.

# CHAPTER 1

## INTRODUCTION

### 1.1 Historical overview

Although predicted by Mendeleev, the element Ge of the IVa column of the periodic table was only discovered by Winkler in 1886 (Claeys and Simoen, 2007), some 125 years ago and 66 years later than silicon. While Ge was the key substrate material used during the early days of the semiconductor transistor and integrated circuit developments, it was later completely overruled by silicon. One can clearly state that the road to silicon was paved with germanium.

The invention of the semiconductor transistor happened accidentally by Shockley, Bardeen and Brattain (Bardeen and Brattain, 1949), while on the search for the field-effect device. In the late forties of the 20th century, germanium was the material of choice, as it was available with the best crystalline quality achievable at that time (Teal et al., 1951). The first point contact transistor fabricated in 1948 by researchers from Bell Labs, the Ge slab, into which a plastic wedge presses two strips of gold foil, is about half a centimeter long. Needless to say that scientifically and technologically this discovery is one of the most important ones of the 20th century. It paved the way to what is currently the largest industry worldwide, namely, the Microelectronics Industry, so that the semiconductor content of electronic systems will be about 25%. Microelectronics products have enabled the Internet revolution, provide for global communication and are expected to play an important role in future health care, automotives and our daily life.

Nowadays, germanium and some derived chemicals ( $\text{GeO}_2$  and  $\text{GeCl}_4$ ) are key materials for a wide variety of applications. The main applications of bulk single

crystalline germanium are lenses and windows for infrared (IR) optics (thermal vision), detectors for gamma radiation and substrates for III-V based optoelectronic devices.

Over the last two decades, germanium has regained a lot of interest as a semiconductor material for optoelectronic and electronic applications. Germanium and gallium arsenide show only a slight lattice mismatch, therefore germanium fulfills one of the main criteria to be considered as a substrate for epitaxial III-V growth.

Additionally, Ge substrates offer certain advantages over those of GaAs such as high crystallographic perfection, high mechanical strength and recycling. These factors have led to the wide use of Ge wafers as substrate of GaAs/Ge solar cells for telecommunication satellites (Derluyn et al., 2003). The use of Ge instead of GaAs has been feasible for the fabrication of magnetoresistive sensors, high electron mobility transistors (HEMTs) (Thomas et al., 2005), and laser diodes (D'Hondt et al., 1998).

Recently germanium regained a lot of attention in the semiconductor industry since it has attractive properties that can provide solutions for some of the major roadblocks that silicon technology currently faces in the development of advanced nanoscale transistor structures. Among these is the continuous scaling down of transistor dimensions driven by the electronics industry striving for higher performance at lower cost per function.

The high mobility of charge carriers in germanium (two times higher than Si for electrons, four times for holes) makes this material ideally suited as channel material for the formation of high-speed circuits where it can potentially provide improved performance in comparison with advanced strained silicon layers.

The high absorption coefficient of germanium compared to silicon in the wavelength range 800-1550 nm, combined with its high carrier mobilities make the material a viable candidate for integration of optical detectors and modulators on complementary-metal-oxide-semiconductor (CMOS) circuits for optical interconnection (Dosunmu et al., 2004). Also for this application germanium can pave the way for integration of III-V optical devices with Si-based electronics, since high-quality epitaxial GaAs can be grown directly on Ge.

Today, single crystals grown by the Czochralski technique provide the closest to perfect germanium material, and are indispensable for a variety of applications. Moreover, it is the material of choice for fundamental scientific research on its physical material parameters.

The use of bulk germanium wafers for the above mentioned new applications in CMOS transistors and optical interconnects is restricted due to problems related to the high density of germanium and hence the high weight of bulk wafers, to their fragility compared to silicon and to the relatively high price of germanium. Therefore, alternative solutions are being developed: epitaxial growth of germanium on a silicon substrate, and the transfer of a germanium layer from a bulk substrate onto an oxidized silicon wafer (germanium-on-insulator).

Although Si is a predominant material in use, it has the disadvantage that its high indirect bandgap prevents sufficient light detection in the standardized frequency bands of telecommunication. The maximum detectable wavelength for Si detectors is 850 nm. Ge, on the contrary, exhibits a higher absorption coefficient ( $\alpha$ ) in this frequency range, and is used for optical communication at near infrared wavelengths which are preferable for fiber optical systems. Again Ge is

advantageous for the utilization in photodetectors as it is compatible with the Si technology platform with higher cost efficiency (Samavedam, 1998).

Both Si and Ge are indirect semiconductors, and therefore have a poor absorption directly above the band gap, but the absorption curve of Ge is much steeper for energies slightly above the band gap. This is caused by the short energetic distance to the first direct transition, which is slightly above the indirect transition (0.2 eV). For Si the next direct transition is far above the indirect one (1.12 eV).

In summary, the absorption is 50 times larger for Ge than for Si for the visible and NIR (Near Infra Red) range, and several orders of magnitude for lower energies (850 nm-1500 nm). The above mentioned higher charge mobilities in Ge allow short detector transit times as well as high speed operation at 850 nm (Akatsu et al., 2006). It has been also reported that a Ge detector could be operated at 40 GHz, and proposed to operate at even beyond 100 GHz (Oehme et al., 2007). In terms of nanostructure dimensions, a Ge quantum dots photodetector has recently been developed and operated with ultra low dark current and high responsivity at around 1.55  $\mu\text{m}$  wavelength (Xu et al., 2014).

## **1.2 Problem statements**

In this study, several problems are essentially addressed and are summarized as follows:

Researchers usually use advanced technology to grow Ge and  $\text{GeO}_2$  nanostructures under certain conditions including vacuum and high temperatures. Growth of Ge and  $\text{GeO}_2$  nanostructures were accomplished in this work using simple electrochemical deposition technique at room temperature. To ease growth manipulation, Ge was prepared in ions form. In order to obtain structure with variety

of morphologies such as microflowers, microspheres, nanowires and nanorods arrays, the electrochemical deposition (ECD) was controlled by a suitable applied current. The advantage of this technique is its potential to obtain thick Ge layer of several microns which is desirable for many applications.

Previous studies showed that the growth of Ge and GeO<sub>2</sub> nanostructures by ECD technique requires complex materials and catalysts (Al-Salman et al. 2008; Zhang et al. 2014). However, in this work the electrolyte solution and the ECD cell used for preparing such structures were simplified and free of catalysts.

Due to the quantum confinement effects the energy bandgap of the nanocrystal is much higher than the bulk crystal, thus Ge nanostructures are candidate for UV detector and GeO<sub>2</sub> nanostructures are promising material for applications in photodetection and gas sensing.

### **1.3 Research objectives**

1. To investigate the effect of different current densities, different durations and type of substrates in synthesizing Ge nanostructures on Si and porous silicon (PS) by ECD technique.
2. To synthesize GeO<sub>2</sub> nanostructures on PS by ECD technique and to study the morphological, structural and optical properties of GeO<sub>2</sub> at different current densities.
3. To examine the Pd/Ge-like microflowers and Pd/GeO<sub>2</sub> nanostructures as photodetector and gas sensor.

#### **1.4 Originality of the research work**

1. In this work, an alternative method to synthesize high quality Ge nanostructures on Si and PS such as, microflowers, microspheres, nanowires and nanorods arrays by ECD technique was suggested.
2. Nonconventional method to synthesize high quality hexagonal GeO<sub>2</sub> nanostructures on PS by using ECD technique was adopted.
3. Fabrication of novel devices based on hexagonal GeO<sub>2</sub> nanostructures for photodetection and gas sensing.

#### **1.5 Outlines of the thesis**

The content of this thesis covers six chapters which are organized as follows:

Chapter one is devoted to an introduction which presents a historical background on Ge and its favorable properties on other semiconductor elements to be used as optoelectronic device in microelectronics industry.

Chapter two includes an overview on semiconductor and Ge nanostructures and their future development. A review on Ge growth techniques is also reported. A brief explanation of the fundamental of electrochemical deposition principles is discussed. Furthermore, the reaction mechanisms to form Ge and GeO<sub>2</sub> nanostructures by ECD are discussed. Finally, the characteristics of Ge photodetector and GeO<sub>2</sub> hydrogen gas sensor are briefly described in this chapter.

Chapter three describes samples preparation of the Ge and GeO<sub>2</sub> nanostructures with various conditions. The general instruments that were used in this study are also summarized. The measurements of current-voltage characteristics and fabrication of various types of devices based on Ge and GeO<sub>2</sub> nanostructures are presented too.

Chapter four covers the results of synthesis and characterizations of Ge nanostructures by ECD technique under different current densities and different durations. Comparative study between the growth of Ge nanostructures on PS and Si substrates is elaborated. In addition, the effect of thermal annealing on the electrical properties of MSM photodetector based on Ge-like microflowers grown on Si as a photodetector under dark, white light and UV illumination is investigated. Apart from that, the photoresponse time of MSM photodetector based on Ge-like microflowers prepared by electrochemical technique for photodetection is also evaluated.

Chapter five discusses the results obtained from the synthesis and characterization of  $\text{GeO}_2$  microstructures grown on PS substrate by ECD. The morphological, structural and optical properties of this resulting film are reported. A comparative study of MSM UV detector based on Ge and  $\text{GeO}_2$  microstructures grown on PS is demonstrated. Finally, the study of the novel gas sensor device for hydrogen based on Schottky barrier of Pd/ $\text{GeO}_2$  microstructures grown on PS by ECD is discussed.

Chapter six is concerned with the conclusions and proposals for future works.

## CHAPTER 2

### LITERATURE REVIEW AND THEORETICAL BACKGROUND

#### 2.1 Introduction

In this chapter, relevant literature reviews, general principles and theories of subjects involved in this work were discussed such as overview of semiconductors nanostructure, fundamental of group-IV elemental semiconductors, crystal structure and physical properties of Ge. Apart from that, principles of electrochemical deposition technique as well as mechanism of the reactions to form Ge and GeO<sub>2</sub> nanostructures by ECD technique were also discussed. Subsequently, the fabrication and characterization of various devices such as MSM UV photodetector and hydrogen gas sensor are addressed.

#### 2.2 Overview of semiconductors nanostructure

Nanoscience and technology are advancing at a rapid pace and making revolutionary contributions in many fields including electronics, materials science, chemistry, biology, mechanics, and optoelectronics. Although nanoscience and technology are progressing along many fronts, the most impressive progress has been witnessed in the area of semiconductor.

Advanced semiconductor growth techniques including molecular beam epitaxy (MBE) and metalorganic chemical vapor deposition (MOCVD), allow fabrication of various semiconductor nanostructures or low dimensional structures. These structures include (i) quantum wells (QWs); where the charge carriers are confined along the growth direction  $z$  but free to move in the other two directions  $x$  and  $y$ , (ii) quantum wires, where the charge carriers are confined in two directions

and only allow one dimensional motion, and (iii) quantum dots (QDs); where the charge carriers are confined in all three directions.

Strong interband transitions are possible in these low dimensional structures because there is a probability of a strong overlap between the wave functions of the electrons and holes. Figure 2.1 compares the density of states as a function of energy in different dimensional materials, bulk, quantum well, quantum wire and quantum dot.

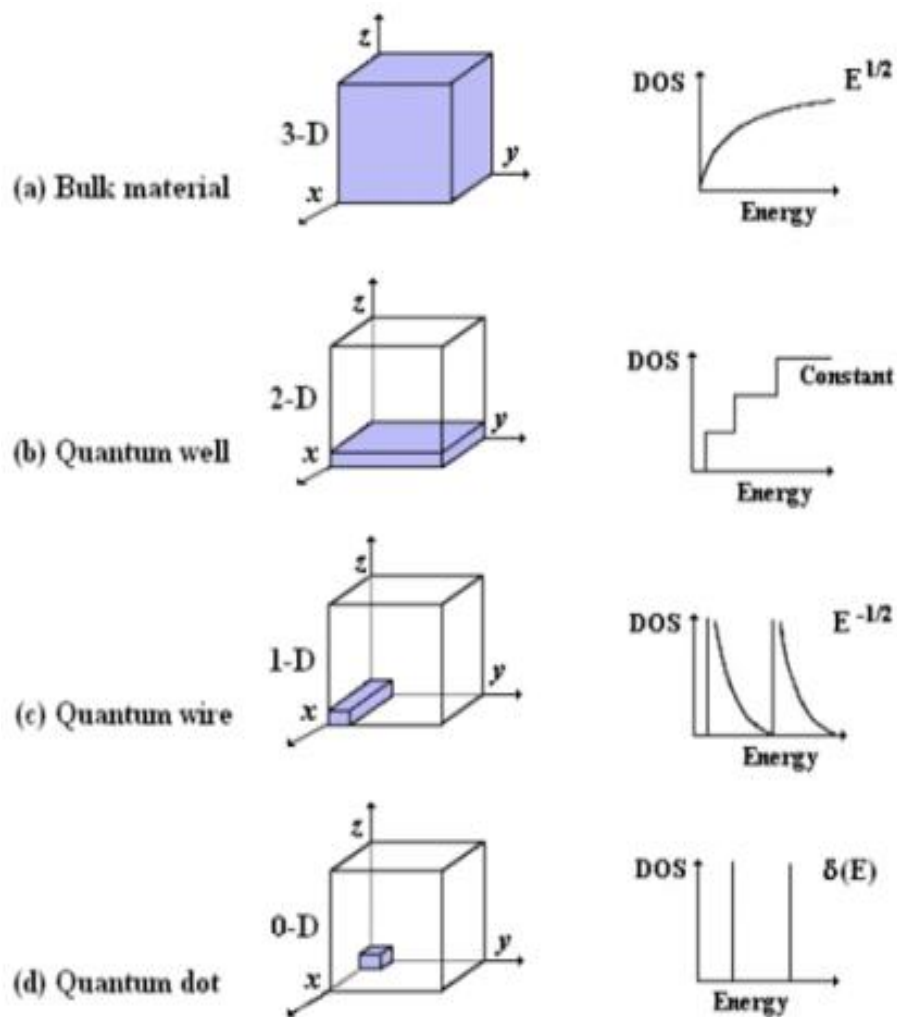


Figure 2.1: Schematic of the low-dimensional structure and the density of state (DOS) as a function of the energy for a particle controlled to move in the bulk (a), in a quantum well (b), in quantum wire (c), and quantum dot (d) [adopted from Hens et al., 2002].

In a quantum well system, due to the one dimensional confinement of electrons, the electron energy levels  $E_n$  can be calculated by Schrödinger equation for an infinitely deep potential well:

$$E_n = \frac{\hbar^2 \pi^2}{2m_e^* L^2} n^2 \quad n = 1, 2, 3, \dots \quad (2.1)$$

where  $m_e^*$  is the effective mass of the electron,  $\hbar$  is Plank's constant divided by  $(2\pi)$ . The dependence of the energy levels on  $1/L^2$  is the quantum size effect or (L is the well width). The dispersion relation of the conduction band for confinement in the z direction can be written as:

$$E(k) = E_c + E_{nz} + \frac{\hbar^2 (k_x^2 + k_y^2)}{2m_e^*} \quad (2.2)$$

where  $E_{nz}$  is given by Eq. 2.1. For the conduction band, the density of states per unit area in a two-dimensional QW system in the subbands (for energies greater than  $E_c + E_{nz}$ ) can be expressed as:

$$g(E) = \frac{m_e^*}{\pi \hbar^2} \quad (2.3)$$

Thus, for each quantum number  $n_z$ , the density of states is constant and the overall density of states is the sum of these values of  $n_z$  which results in a staircase-type distribution with a step height given by Eq. 2.3.

In a one-dimensional quantum wire system, the carriers are confined in two directions; z and y as shown in Figure 2.1 (c), and the dispersion relation of the conduction band can be written as:

$$E(k) = E_c + E_{nz} + E_{ny} + \frac{\hbar^2 k_x^2}{2m_e^*} \quad (2.4)$$

In each of the subbands, the density of states can be described as a function of energy by  $g(E) \propto E^{-1/2}$

In a zero-dimensional quantum dot system, the carriers are confined in three directions; the dispersion relation of the conduction band can be expressed as:

$$E(k) = E_c + E_{nz} + E_{nx} + E_{ny} \quad (2.5)$$

Thus, QDs are generally referred to as artificial atoms due to the similar discrete energy level structures. It is noteworthy that the density of states in the valence band has a similar distribution to the one in the conduction band. As a result of quantum confinement in the different directions, there is a change in the wave function describing the behavior of the electrons and holes, and consequently the number of states per unit energy, i. e. the density of state (DOS), changes as a function of the energy  $E$  of the particle, as illustrated in Fig. 2.1.

Nanostructured materials are those with at least one dimension falling within the nanometer scale. These include nanoparticles, nanorods, nanowire, and thin films. Recently, nanostructured materials have received much attention from researchers because of their unique physical and chemical properties that are widely different from those of their bulk phases. Their properties are strongly dependent on the structure type, dimension, and surface nature. Understanding how the properties of nanostructures change with these parameters is necessary. Controlling the properties of these materials by varying these parameters can be done for technological applications such as optoelectronics and sensing (Berry, 1967; Dingle et al., 1974).

The ability to tune the optical absorption/emission properties of semiconductor nanostructures by varying its structure size is especially attractive in

bandgap engineering of materials. Furthermore, quantum confinement effects are expected to lead to a change in the density of states of electrons, phonons, and in the mechanism rates of charge carrier electron-hole pair (e-h) recombination (Fendler and Meldrum, 1995; Ledentsov et al., 1996; Smith and Doline, 1992).

Semiconductor nanostructures have been enabled by the advancements in epitaxial growth techniques, which are now capable of growing epilayers as thin as one atomic layer and with interface roughnesses that are a mere fraction of a monolayer. The development of advanced crystal and thin film growth technologies capable of realizing high crystalline quality and purity of materials are enabling steps in bringing semiconductor devices to reality.

All semiconductors can be classified either as direct gap semiconductors with a valence band maximum and a conduction band minimum occurring at the same point in the Brillouin zone such as ZnO and GaN, or as indirect gap semiconductors in which these extrema occur at different points in the Brillouin zone such as Si and Ge. The optical properties of direct gap semiconductors differ considerably from those of indirect gap semiconductors (Yacobi, 2003).

The quantum size effect due to three-dimensional confinement is obvious when the microcrystal size is less than the exciton effective Bohr radius. Since Ge has smaller electron and hole effective masses and a larger dielectric constant than silicon (Si), the effective Bohr radius of the excitons in Ge is larger than that in Si. This implies that the Ge microcrystals show a larger shift of an optical bandgap (blue shift) than the Si microcrystals (Maeda, et al., 1991).

Quantum confinement describes the increase in energy which occurs when the motion of a particle is restricted in one or more dimensions by a potential well. As the confining dimension decreases, the energy of particles increases. A crystal

nanoparticle is treated as a well that is confined in all three dimensions. Therefore, the energy bandgap of the nanocrystal is much higher than the bulk crystal (Brus, 1983). Maeda et al. (1991) reported the first observation of visible photoluminescence (PL) of Ge microcrystals embedded in SiO<sub>2</sub> glassy matrices prepared by an rf-magnetron co-sputtering method. They ascribed the visible luminescence peak at 2.18 eV to quantum confinement of electrons and holes.

Min et al. (1996) observed a strong red (1.8 eV) PL of Ge nanocrystals in SiO<sub>2</sub> films made by Ge ion implantation. However, the measured PL peak energy and lifetimes showed poor correlations with nanocrystal size, compared to calculations involving radiative recombination of excitons in germanium. This observation suggested that the red PL was not due to the radiative recombination of excitons confined in Ge nanocrystals. Rather, the author suggested that the origin of this red PL was the radiative defect centers in the SiO<sub>2</sub> matrix.

Later, many reports showed that the PL of Ge-doped silica occurs in the visible range. The observed PL was mainly in three visible ranges, red (1.8 eV), green-orange (2.2-2.3 eV), and blue-violet (3.0-3.1 eV) (Zhang et al., 1998; Kartopu et al., 2003; Ortiz et al., 2005).

### **2.3 Overview of Ge nanostructure growth techniques**

Germanium properties are essentially significant for the growth techniques of thin layers. For the last two decades a number of research studies has been carried out in such context. Epitaxial growth of Ge is the most common method which includes chemical vapor deposition (CVD), molecular beam epitaxy (MBE), and atomic layer deposition (ALD) as well as the electrochemical deposition (ECD) technique.

### 2.3.1 Chemical vapour deposition (CVD)

In CVD, a mixture of the precursor gases is diluted in a carrier gas (usually H<sub>2</sub>) and injected into a chamber, heated by radio frequency, infrared lamps or a resistance heater. The substrate is placed over a graphite susceptor in the hot zone of the reactor. The precursor gases decompose after reaching the high temperature region and deposition occurs. The conditions of the flow dynamics, the chamber geometry, the precursor partial pressure and the operating pressure must be carefully chosen in order to promote an ordered deposition onto the substrate.

A standard CVD with GeH<sub>4</sub> on Si substrate is usually performed at a temperature between 300 and 500°C. A wide range of reactor pressures is reported in the literature, ranging from UHV (10<sup>-8</sup>-10<sup>-7</sup> bar) to atmospheric pressure. A general feature of Ge/Si heteroepitaxy is island formation due to lattice mismatch, and a modified Stranski-Krastanov mechanism occurs. Kaminis et al. (1997) observed an initially pseudomorphic coverage up to 3.5 Ge monolayer followed by nucleation of islands with a constant aspect ratio (11:1 between diameter and height).

The size and shape of the islands and their dimension and homogeneity depend on growth conditions, growth temperature and on the alloy composition (Cunningam et al., 1991), while nucleation is critically dependent on surface purity and physical perfection involving steps and substrate misorientation (Mo and Lagally, 1991).

Epitaxial growth of Ge was observed on Ge (100) surfaces by using a GeCl<sub>4</sub>H<sub>2</sub> gas system at temperature range of 490-565°C under relatively low GeCl<sub>4</sub> partial pressures less than  $2 \times 10^{-3}$  torr. It was reported that the surface reaction takes place between two hydrogen atoms dissociatively adsorbed and a surface-adsorbed GeCl<sub>2</sub> molecule. GeCl<sub>2</sub> molecules adsorbed on the surface are formed directly from

GeCl<sub>4</sub> molecules, not through gas-phase reduction by hydrogen (Ishii and Takahashi, 1988).

A rapid thermal chemical vapor deposition was carried out to grow Ge layer on Si substrates. Results showed uniformity of the thickness and good quality Ge layer with a homogeneous distribution of tensile strain. The surface morphology was very smooth. (Ho Kil et al., 2014).

### **2.3.2 Molecular beam epitaxy (MBE)**

MBE is recognized as a technique used for preparing high quality layers, superlattices and heterostructures with excellent thickness control, composition uniformity, and sharp dopant profiles. The term “beam” is used because the process takes place in ultra-high vacuum chamber, and thus the mean free paths of the source materials vapors are sufficiently large to prevent all atomic interaction before arriving at the substrate. These vapors are from element sources with high purity which are slowly heated in individual quasi-Knudsen cells, and released into the vacuum chamber by computer-controlled shutters. Upon condensation onto the single crystal substrate, the elements from the vapors start to interact with each other as well as with the substrates, and then atomic layers are epitaxially grown one layer at a time. The crystal quality and layer thickness can be monitored by reflection high energy electron diffraction (RHEED) during the crystal growth.

MBE was historically the first technique used for the deposition of SiGe layers (Kasper et al., 1975) and is still a widely used research tool for fundamental studies and for designing novel device structures, even if it is not widely employed in production lines. Eaglesham and Cerullo (1990) used the RHEED in MBE deposition equipment to explain island growth in term of elastic deformation around the islands

which accommodate the mismatch where a 50 nm thick dislocation free Ge islands on Si were obtained.

A Ge microstructure was recently deposited on PS under various experimental conditions (Gouder et al., 2014). The morphology and structure of Ge layers were investigated by transmission electron microscopy, high resolution X-Ray diffraction and atomic force microscopy as a function of the deposition temperature and deposited thickness. The results showed that the surface roughness, level of relaxation and Si-Ge intermixing depend on the growth temperature and deposited thickness. When deposited at temperature  $>500$  °C, the Ge layers were fully relaxed with a top  $\text{Si}_{1-x}\text{Ge}_x$  layer  $x = 0.74$  and a very flat surface.

### **2.3.3 Atomic layer epitaxy (ALE)**

Atomic layer epitaxy (ALE) has become a very common technique for fabricating microelectronic devices (Goodman and Pessa, 1986; Suntola and Hyvarinen, 1985). By this method the epitaxial growth takes place in a layer by layer self-limiting process, and precise control of thickness and film composition is possible. In an ALE process the growth occurs in separate steps: the precursor is firstly adsorbed on the substrate surface and then the supply is switched off. A purge step follows, to desorb and remove the reaction by-products. This technique is usually adopted for binary or ternary compounds in order to have precise control of the stoichiometry and to avoid parasitic reactions between the different species. For this reason, ALE of elemental semiconductors such as Ge has not been the object of wide interest, but there are several works concerning the preparation of Ge films using this technique (Tillack and Yamamoto, 2009; Sugahara et al., 1994).

Takahashi et al. (1989) proposed a process for Ge ALE using diethyl germane  $\text{GeEt}_2\text{H}_2$  ( $\text{Et} = \text{C}_2\text{H}_5$ ) in which a monolayer of  $\text{GeEt}_2$  is formed through a precursor surface reaction after deposition at low temperature. The adsorption of  $\text{GeEt}_2$  is self limiting and a single Ge monolayer should be formed. After a gas purge, the ethyl groups are desorbed by increasing the temperature. A clean Ge monolayer growth was achieved and layer by layer Ge deposition was obtained. This technique is based on the repetition of a sequential process consisting of gas introduction on the Ge surface at  $220^\circ\text{C}$ , gas evacuation, and Et group desorption at temperatures over  $400^\circ\text{C}$ .

#### **2.3.4 Electrochemical deposition (ECD)**

Electrochemical deposition has become an attractive method, where one can put a coating of one material on another simply by donating electrons to ions in a solution and the studies of the process at an atomic level continue to yield surprises. Electrochemical deposition is exceptionally versatile, and many valuable applications are being explored. Comparing to other techniques, the advantages of ECD are as follows: the thickness and surface morphology can be controlled by growth parameters, the deposition rate is relatively high, the experimental setup is considerably of low cost, it is a low temperature process and it makes the doping of the impurities easy (Katayama and Izaki, 2000; Gu and Fahidy, 1999; Izaki and Omi, 1996).

ECD, which has been widely used for metal or metallic alloys, was used recently for semiconductors as a new challenge for both academic and economic view points. However, the application of the ECD technique to semiconductors has been limited until recently, mainly because of complexities in the electrodeposition

of semiconductors and the stringent materials property requirements for device applications. Research and development in the area of semiconductor electrodeposition have been continued after the pioneering work by Kröger (1978) and Panicker et al. (1978). They found that both n- and p-type polycrystalline CdTe layers could be produced by cathodic electrodeposition using acidic sulfate electrolytes containing  $\text{Cd}^{2+}$  and  $\text{HTeO}^{2+}$  ions. Afterwards, other semiconductor compounds such as  $\text{CuInSe}_2$  and  $\text{CuInS}_2$  have been synthesized by ECD technique (Oliveria et al., 2002; Pottier and Maurin, 1989; Mishra and Rajeshwar, 1989).

Many research groups have extensively investigated and studied the ECD of the compound semiconductors. Bhattacharya (1983) was the first to report the synthesis of  $\text{CuInSe}_2$  by ECD. An aqueous solution containing Ga and As ions in proper ratios was used to prepare GaAs films using an electrodeposition technique at low current (Chandra and Khare, 1987).

De Mattei et al. (1978) carried out the ECD of GaP from a solution containing sodium metaphosphate, NaF, and  $\text{Ga}_2\text{O}_3$ . The preparation of thin films of ZnTe was first reported by Basol and Kapur using two-stage process involving ECD of Te and Zn stacked layers from aqueous electrolytes followed by annealing (Basol and Kapur, 1988). ECD of ZnO has initially been introduced by Pauporte and Lincot (1999), and also Peulon and Lincot (1996).

ECD of Ge is still in the beginning. Reports on using ECD to grow Ge thin film are limited. Macroscopically thick and amorphous Ge films can be obtained from  $\text{GeI}_4$  dissolved in propylene glycol at elevated temperature under galvanostatic conditions (Fink and Dokras, 1949). Szekely (1951) showed that roughly 130  $\mu\text{m}$  thick Ge layer was electrodeposited from  $\text{GeCl}_4$  dissolved in propylene glycol at  $59^\circ\text{C}$  and a constant current density of  $0.4 \text{ mA/cm}^2$ . Ge can also be electrodeposited

in high temperature molten salts (Monnier and Tissot, 1964). Endres (2001) presented detailed ECD of Ge from  $\text{GeI}_4$  dissolved in room temperature ionic liquid 1-butyl-3-methylimidazolium hexafluorophosphate, so that elemental Ge can be deposited via several steps of which two-dimensional islands are formed which are likely to be composed of subvalent germanium species.

Freyland et al. (2003) also demonstrated an ECD of Ge on Au (111) and Si (111) in liquid  $[\text{BMIm}]^+ \text{PF}_6^-$  saturated with  $\text{GeCl}_4$  or  $\text{GeBr}_4$  at room temperature and showed first investigation of ECD of ultrathin Ge films with varying thickness on Au (111) and Si (111). By probing the electronic structure of these films through in situ scanning tunneling spectroscopy (STS) spectra, a metal-semiconductor transition was indicated with increasing film thickness above 2-3 nm. A comparison of these results with ultrathin Ge films grown by epitaxial vapour deposition is also presented.

Al-Salman et al. (2008) showed that nanosized Si, Ge and, for the first time,  $\text{Si}_x\text{Ge}_{1-x}$  films could be made at room temperature by a relatively simple electrochemical process (compared with ultra high vacuum techniques) in the air- and water-stable ionic liquid  $[\text{Py}_{1,4}]\text{Tf}_2\text{N}$  containing  $\text{GeCl}_4$  and/or  $\text{SiCl}_4$  as precursors. The composition, thickness and morphology of the deposit can be modified by simply changing the electrochemical parameters like concentration and electrode potential. The  $\text{Si}_x\text{Ge}_{1-x}$  deposited showed a strong color change (from red to blue) at room temperature during electrodeposition, which is likely to be due to a quantum size effect. The observed colors are indicative of bandgaps between at least 1.5 and 3.2 eV.

The electrodeposition of Ge thin films on n-silicon Si (100) was reported by Zainal Abidin et al. (2013). With constant current of 50 mA for 30 min, the measured Raman spectra and electron backscattering diffraction images show that the as-

deposited Ge thin film was amorphous. The crystallization of deposited Ge was achieved by rapid thermal annealing at 980°C.

## 2.4 Properties of Ge

### 2.4.1 Crystal structure of Ge

Germanium crystallizes in a diamond lattice structure which is part of the cubic crystal family. The diamond lattice structure can be seen as two interpenetrating face centered cubic (fcc) sublattices with one sublattice displaced

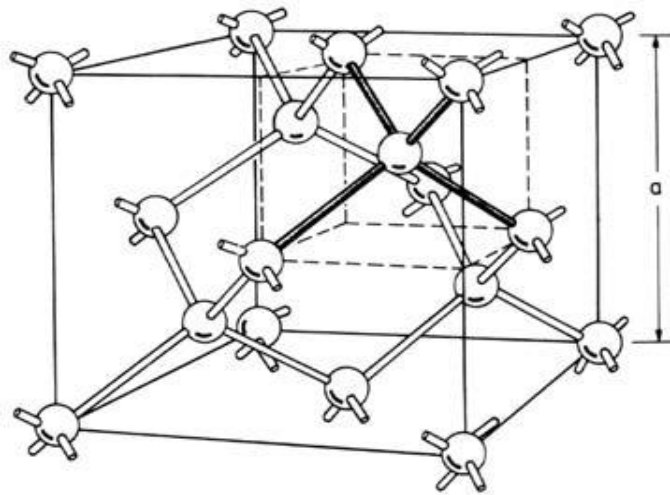


Figure 2.2: Diamond lattice structure [adopted from Sze, 1985].

from the other by one quarter of the distance along a diagonal of the cube (i.e. a displacement of  $\sqrt{3}/4$ ). Within this structure all atoms are identical and each of them is surrounded by four equidistant nearest neighbors lying at the corners of a tetrahedron as shown in Figure 2.2. Ge has four electrons in the outer shell and that the element makes a covalent binding because each atom shares its valence electrons with its four neighbors. This binding occurs between atoms of the same element or

between different atoms that have similar outer-shell electron configurations, e.g. silicon and germanium atoms (Sze, 1985).

The orientation and properties of the crystal planes are important because most semiconductor devices are built on or near the semiconductor surface. A convenient method for the definition of the various planes in a crystal is the use of Miller indices. These indices are determined by, first, finding the intersection of the plane with the three axes with respect to the lattice constant, and then taking the reciprocal of these numbers and further reduce them to the smallest possible three integers by keeping the same ratio. The result is enclosed in parentheses  $(h k l)$  called Miller indices for a single plane or a set of planes  $(h k l)$ . Figure 2.3 shows the Miller indices of the most important planes in a cubic crystal.

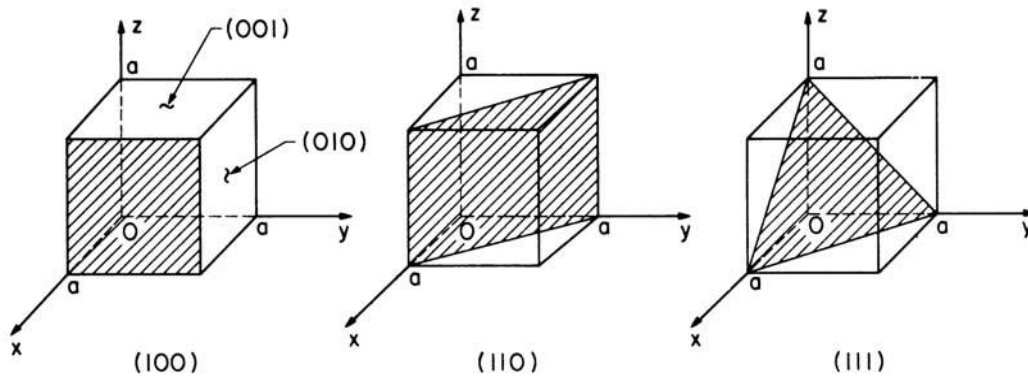


Figure 2.3: Miller indices of some important planes in a cubic crystal [adopted from Sze and Ng, 2008].

Germanium has an indirect band gap of 0.66 eV at 300 K, which increases to 0.74 eV at 1.5 K. The conduction band minimum lies in the  $[111]$  directions at the L point. The intersection point with the  $[111]$  direction is called L; the line  $\Gamma$ -L is called  $\Lambda$ . The L minimum is four-fold degenerate. The surfaces of constant energy (Figure 2.4) are rotational ellipsoids, with a longitudinal effective mass of  $m_l^* = 0.64 m_0$  and a transversal effective mass of  $m_t^* = 0.08 m_0$ .

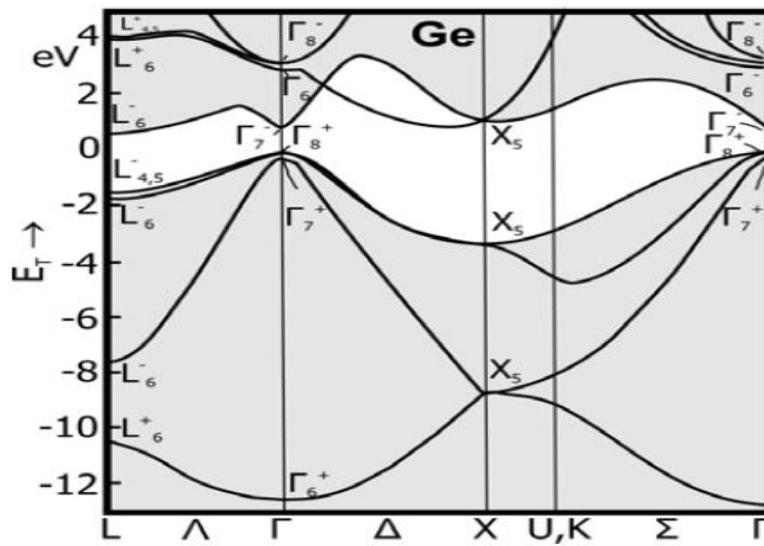


Figure 2.4: Band structure of germanium [adopted from Sze, 1985].

The hole bands are two-fold degenerate at their maximum at the  $\Gamma$  point. The degeneration corresponds to an average heavy hole mass of  $0.28 m_0$  and an average light hole mass of  $0.043 m_0$  (Kasper, 1995).

### 2.4.2 Physical properties of Ge

Elementary germanium is a silvery white metal having much the outward appearance of bright solder when fused. This appearance is deceptive, however, since germanium is very hard and has a tendency to fracture when drilled or cut. When germanium is fractured, the break is shiny and hard, similar to that of metallic silicon. Like bismuth and gallium, the metal expands on freezing. Some physical constants of Ge are summarized in Appendix A.

### 2.4.3 Germanium dioxide ( $\text{GeO}_2$ ) properties

Germanium dioxide ( $\text{GeO}_2$ ) is a chemical compound which can appear at ambient temperature in two predominant polymorphs; hexagonal and tetragonal as

crystalline structure. Also, there is a third form in which  $\text{GeO}_2$  occurs and that is the glassy amorphous which is similar to fused silica. In many respects, both  $\text{GeO}_2$  and  $\text{SiO}_2$  are identical. In its nanoscale dimensions,  $\text{GeO}_2$  possesses a number of unique properties including wide bandgap energy in the order of 5 eV (Zhang et al., 2014), higher refractive index value in the range of 1.6 to 1.65 as compared to around 1.45 for the silica glasses and high mechanical strength (Chiu and Huang, 2009). Moreover, it has linear coefficient of thermal expansion higher than that of silicate glass, high thermal stability and specific capacity which is the amount of charge that can be stored in a unit mass. The value of this specific capacity has been reported as  $1120 \text{ mA h g}^{-1}$  which is three times higher than that of graphite (Ngo et al., 2014). Also, it is characterized with high dielectric constant as well as the exhibition of visible light photoluminescence.

According to the properties mentioned above,  $\text{GeO}_2$  is widely used in the following fields:

- Gas sensing (Wang et al., 2010)
- An attractive host for optical impurities to develop luminescent devices from the ultraviolet-blue to the near-infrared range (Hidalgo et al., 2009)
- Anode material in Li batteries (Ngo et al., 2014)
- Thin films of  $\text{GeO}_2$  are used in optical waveguides for integrated optical systems and nanoconnections in optical devices (Pei et al., 2009)
- Energy storage capacitors because of the high dielectric constant (Murphy et al., 2014)
- Optical filter elements (Vega et al., 1994)

Having discussed the properties and fields of applications of  $\text{GeO}_2$ , it is convenient to mention the methods for preparing its nanostructures. These technique

include radio frequency magnetron sputtering (Chiasera et al., 2013), laser ablation (Vega et al., 1994), sol-gel deposition (Hsu et al., 2011), reactive thermal evaporation (Murad et al., 2012), electron-beam evaporation (Krupanidhi et al., 1984), Plasma Enhanced Chemical Vapor Deposition (Reich et al., 1990), reactive DC magnetron sputtering (Lange et al., 2000), and the ECD technique with which this thesis is partly concerned to grow  $\text{GeO}_2$  on PS.

## **2.5 Principles of electrochemical deposition (ECD) technique**

Electrochemical deposition has typically been used for the plating of metals and the art has historically been developed industrially, mainly by experience. Research has deepened the understanding of the deposition processes and ECD today provides many exciting routes for the synthesis of metal, metal oxides, alloys, semiconductors and nanostructured materials. Fundamental aspects of ECD include the heterogeneous electron transfer step between the electrode and the electroactive species present in the solution as well as the transition of the discharged material atoms into the crystalline state (Raub and Müller, 1967).

The deposition is carried out in an electrochemical cell consisting of a reaction vessel and two or three electrodes. In the two-electrode cell, the reactions are controlled by the current applied between a working electrode (substrate) and a counter electrode. In the three-electrode cell (Figure 2.5) a reference electrode is used to control or measure the potential of the working electrode, and deposition is carried out by controlling either the current or the potential due to the mode of operation. For two electrodes cell the ECD of materials is commonly carried out galvanostatically, i.e., with a constant current applied between the electrodes. No reference electrode is needed which makes the galvanostatic system very practical